 CMC, vol.36, no.1, pp.73-97, 2013

Multivariate Adaptive Regression Splines Model to Predict Fracture Characteristics of High Strength and Ultra High Strength Concrete Beams

P. Yuvaraj[1], **A. Ramachandra Murthy**[2], **Nagesh R. Iyer**[3], **Pijush Samui**[4], **S.K. Sekar**[5]

Abstract: This paper presents Multivariate Adaptive Regression Splines (MARS) model to predict the fracture characteristics of high strength and ultra high strength concrete beams. Fracture characteristics include fracture energy (G_F), critical stress intensity factor (K_{IC}) and critical crack tip opening displacement ($CTOD_c$). This paper also presents the details of development of MARS model to predict failure load (P_{max}) of high strength concrete (HSC) and ultra high strength concrete (UHSC) beam specimens. Characterization of mix and testing of beams of high strength and ultra strength concrete have been described. Methodologies for evaluation of fracture energy, critical stress intensity factor and critical crack tip opening displacement have been outlined. MARS model has been developed by establishing a relationship between a set of predicators and dependent variables. MARS is based on a divide and conquers strategy partitioning the training data sets into separate regions; each gets its own regression line. Four MARS models have been developed by using MATLAB software for training and prediction of fracture parameters and failure load.MARS has been trained with about 70% of the total 87 data sets and tested with about 30% of the total data sets. It is observed from the studies that the predicted values of P_{max}, G_F, K_{IC} and $CTOD_C$ are in good agreement with those of the experimental values.

Keywords: High strength concrete; Ultra high strength concrete; Fracture mechanics; Fracture characteristics; Multivariate adaptive regression splines

[1] Bridges department, L&T Ramboll Consulting Engineers Lts, Guindy, Chennai, Tamilnadu, India. E-mail: yuvarajprakash@gmail.com
[2] Senior Scientist, CSIR-SERC, Chennai-113. Email : murthyarc@serc.res.in
[3] Director, CSIR-SERC, Chennai-600113, Tamilnadu, India. Email : nriyer@serc.res.in
[4] Professor, CDMM, VIT University, Vellore, Tamilnadu, India. Email: pijush.phd@gmail.com
[5] Principal, Annamalaiar College of Engineering, Modaiyur, Polur, Tamilnadu, India.

1 Introduction

Concrete has been one of the most commonly used construction materials in the world. One of the major problems civil engineers face today is concerned with preservation, maintenance and retrofitting of structures. The historical development of concrete material may be marked and divided into several stages. The first is the traditional normal strength concrete followed by high strength concrete, high performance concrete and reactive powder concrete/UHSC. Since UHSC is a relatively new material, the fracture behaviour of this material is not well understood (Richard and Cheyrezy 1994, 1995, Mingzhe et al. 2010, Goltermann et al. 1997). Concrete is a quasi-brittle material, which means its fracture process zone (FPZ) size is not small compared with the typical specimen or structural dimension. Classical linear elastic fracture mechanics (LEFM) approach is unable to predict the progressive failure of concrete specimens due to the presence of large FPZ of variable size ahead of the crack tip and the cohesive stress transferred within FPZ of the quasi-brittle materials like concrete (Bazant 2000). The LEFM based modeling approach assumes that once a crack propagates by a distance, this part of the material loses its load carrying capacity suddenly and completely. The complex nonlinear phenomena that take place in FPZ can be idealized and approximated using nonlinear fracture approaches to predict the localized physical behaviour in the vicinity of a crack and at the crack tip. Nonlinear fracture mechanics based approach recognizes that FPZ exists in front of the crack tip, in which the material can still carry loadings by mechanisms such as aggregate interlocking, surface friction and material bonding (Murthy et al. 2010, Bhashya et al. 2011, Murthy et al. 2012, Dong and Atluri 2013). As the crack propagates and opens, the material in FPZ softens with gradual energy dissipation, which can be accurately modeled by the fictitious crack model. The direction of the crack propagation is generally assumed to be perpendicular to the direction of the maximum stress at the crack tip. The cohesive crack model is one of such simplified nonlinear fracture models that can simulate satisfactorily the behaviour of concrete fracture. Inspired by the early stage of development of the fracture models (Barenblatt 1959, Dugdale 1960). Hillerborg et al. (1976) initially applied cohesive crack method (or fictitious crack model) as a suitable nonlinear model for mode I fracture to simulate the softening damage of concrete structures.

This paper adopts Multivariate adaptive regression spline (MARS) for predicting the fracture characteristics and failure load of HSC and UHSC beams. MARS is relatively a new technique used for modeling data depicting non-linear relationship (Friedman 1991). MARS establishes the relationship in non-linear form between the response and predictor variables and identifies the interactions and conditional relationships among the predicator variables. MARS attempts to adapt to the un-

known functional form using a series of multi-linear piecewise regression splines. MARS algorithm involves in the process of eliminating the overfitting of data and other inconsistencies in the data. The MARS approach is capable of detecting interaction among other variables. MARS is based on a divide and conquers strategy, partioning the training data sets into separate regions; each gets its own regression line.

MARS was successfully applied in various fields including biological sciences (Prasad and Iverson 2000) cancer research (Malick et al. 1997), chemical studies (Veaux et al. 1993), communication (Ekman and Kubin 1999), finance (Abraham 2002), Engineering (Jin and Chen 2000) and genetics (York and Eaves 2001).

Riedi (1997) used MARS for modeling segmental duration in speech synthesis for predicting natural sounding durations for German language. Chun et al. (2003) adopted MARS for simulation of pesticide transport in soils and mentioned that using limited training data, MARS can simulate complex physicochemical phenomena. Chou et al. (2004) employed artificial neural network (ANN) and MARS in developing diagnostic techniques that help in identifying breast cancer using a fine needle aspiration cytology dataset. Leathwick et al. (2005) made use of MARS to predict the distribution of New Zealand's freshwater diadromous fish by determining relationship between fish species and different environmental variables. Loizos and Karlaftis (2006) assessed the pavement condition by using ANN and MARS models. Zhou and Leung (2007) predicted object-oriented software maintainability using MARS and mentioned that the MARS is as accurate as the all other models in other cases considered in their investigation. Nii et al. (2009) investigated on doweled pavement performance by using MARS and hyperplanes (HHP) and made a comparative analysis between them. Vidoli (2011) evaluated the water sector in Italy through a two stage method using conditional robust non-parametric frontier and MARS. From the limited available literature, it is observed that MARS is employed in various fields and to the best of authors' knowledge, no research investigations are reported in the field of structural engineering.

This paper presents the details of characterization and casting of high strength and ultra high strength concrete beams. Methodologies for evaluation of fracture characteristics have been explained in brief. Applicability of MARS to predict fracture characteristics of high strength and ultra high strength concrete beams has been examined.

2 Experimental investigations

Three different mixes designated as HSC, HSC1 and UHSC are characterized and their mix proportions have been derived by using appropriate method and several

trials. For HSC, the ingredient materials are Portland cement, coarse aggregate, fine aggregate and water, whereas for HSC1, the materials are Portland cement, silica fume, quartz sand, high range water reducer, water and steel fibers. Further, for UHSC, the materials are Portland cement, silica fume, quartz sand, quartz powder, high range water reducer, water and steel fibers. The main difference between HSC1 and UHSC is the absence of quartz powder in the case of HSC1 mix. Bureau of Indian Standard code has been used for HSC mix design, whereas HSC1 and UHSC mixes have been designed based on the limited literature available and several trials. Several trials have been attempted before arriving at a final mix design. The final mix proportions and ratio obtained are given in Table 1.

Table 1: Mix Proportions for HSC, HSC1 and UHSC

Property	HSC	HSC1	UHSC
Water/cement ratio	0.45	0.33	0.23
Cement, kg/m^3	452.44	811.7	838.93
Silica fume, kg/m^3	-	202.9	209.73
Quartz sand, kg/m^3	-	1217.5	922.82
Quartz powder, kg/m^3	-	-	335.57
Fine aggregate, kg/m^3	565.55	-	-
Coarse aggregate, kg/m^3	1127.01	-	-
Water, kg/m^3	203.6	267.9	192.95
Steel Fiber, kg/m^3		157.20	158.50
Superplasticizer(SP), (% weight of cement content in mix)	-	2.5%	3.5 %

2.1 Specimen Preparation

Preparation, demoulding and curing of HSC specimens is in conventional way, whereas the procedure for specimen preparation for HSC1 and UHSC is outlined below.

- A Hobart mixer machine (15 kg capacity) or Eirich type mixer (150 liter capacity) is used to mix the concrete mixtures.
- Well mixed dry binder powder is then slowly poured in to the bowl while the mixer is rotating at a slow speed.
- The speed of the mixer is increased and the mixing process is continued for about two to three minutes.

- Water is then added.
- Additional mixing is performed at this speed until a uniform mixture is achieved.
- Fibers are added after mixing all the ingredients such as cement, quartz sand, quartz powder and silica fume with water and superplasticizer.
- Fresh mixture is poured in to the moulds using a steel scoop.
- Compaction is done by placing the filled moulds on a laboratory table vibrator for about 2 minutes.
- The specimens are demoulded after a lapse of 24 hours.
- Immediately after demoulding, the specimens are fully immersed in potable water at room temperature for 2 days. After 2 days of normal water curing, the specimens are placed in a autoclave and maintained at 90˚C for 2 days. Further, the specimens are placed in oven and maintained at 200˚C for 1 day followed by autoclave curing.

Mechanical Properties

Various mechanical properties such as compressive strength, spilt tensile strength of HSC, HSC1 and UHSC mix at 28 days are shown in Table 3. From Table 3, it can be observed that the split tensile strength for the case of HSC is 4.0 MPa. It is about 7% of compressive strength. In the case of HSC1, the split tensile strength is about 18% of compressive strength. The increase in strength is large compared to HSC. The increase in strength may be due to various sizes of ingredients and steel fibres. Further, it can be observed from Table 2 that UHSC has high compressive strength and tensile strength. The high strengths can be attributed to the contribution at different scales viz., at the meso scale due to the fibers and at the micro scale due to the close packing of grains, which is on account of good grading of the particles.

Table 2: Mechnanical properties of HSC, HSC1 and UHSC

S. No	Mix ID	Compressive Strength (MPa)	Split tensile Strength (MPa)	Modulus of elasticity (MPa)
1.	HSC	57.14	3.96	35,780
2.	HSC1	87.71	15.38	37,890
3.	UHSC	122.52	20.65	42,987

Casting of Beams

Different beams, namely, small, medium and large size with various notch depths have been cast to study the fracture behaviour. The experimental setup consists of MTS 2500 kN capacity servo hydraulic UTM with online data acquisition system. All the specimens have been tested under displacement control at a rate of 0.02 mm/min. The mid-span downward displacement is measured using linear variable displacement transducer (LVDT), placed at center of the specimen under bottom of the beam. A clip gauge is used to measure the crack mouth opening displacement (CMOD). The data acquisition records load, CMOD, mid-span displacement and time. Appropriate load cells have been used for testing.

3 Fracture Characteristics

Fracture characteristics such as fracture energy (G_F) based on work-of fracture, fracture toughness (K_{IC}) and CTODc - Crack tip opening displacement for HSC, HSC1 and UHSC specimen have been estimated based on the experimental observations. Brief description on the evaluation of G_F, K_{IC} and $CTOD_C$ has been outlined below.

3.1 Fracture energy (G_F)

In general, concrete structures contain voids and flaws. These flaws grow and propagate leading to failure. The fracture energy is one of the important parameter in the analysis of cracked concrete structures. Fracture energy, G_F is an important fracture mechanic parameter to describe the resisting properties of concrete fracture. In fact the fracture energy can be seen as a measure for the ductility of concrete and it is considered as a material parameter. The fracture energy, G_F is defined as the amount of energy necessary to create a crack of unit surface area projected in a plane parallel to the crack direction.

The area under the load-displacement plot is considered as the work of fracture (W_F) and is defined as

$$W_F(w) = \int_0^w P dw \tag{1}$$

where "w" is the crack mouth opening displacement, W_F is the work of fracture, P is the applied load.

According to RILEM method of Hillerborg, the fracture energy G_F is the average energy given by dividing the total work of fracture by the projected fracture area (RILEM 1985, Karihaloo 1995). In case of a specimen of depth d and initial crack

length $a_{0,}$ the fracture energy is given by

$$G_F = \frac{W_F}{(d-a_0)t} \tag{2}$$

d = Depth of the beam, a_0 = Initial crack length, t = Thickness of the beam,
W_F = Area below the measured total load- displacement plot

3.2 Fracture toughness K_{IC} and CTOD$_c$ - Crack tip opening displacement

Critical stress intensity factor (K_{IC}) and critical crack tip opening displacement CTOD$_c$ have been derived from Jenq and Shah effective elastic crack model called the two parameter fracture model (TPFM) (Jenq and Shah 1985). The details are given below:

The TPFM requires at least one cycle to obtain the loading (C_i) and unloading (C_u) compliances, and also the peak load (P_c). The self-weight (P_0) of the specimen is also included. The critical effective elastic crack length (a_c) at the peak load is calculated from the modulus of elasticity obtained with the loading and unloading compliance, E_1 and E_2, respectively.

$$E_1 = \frac{6Sa_0g_2(\alpha_0)}{C_iD^2t}, \tag{3}$$

$$E_2 = \frac{6Sa_cg_2(\alpha_c)}{C_uD^2t}, \tag{4}$$

$$\alpha_0 = \frac{(a_0+HO)}{(D+HO)}, \quad \alpha_c = \frac{(a_c+HO)}{(D+HO)}, \tag{5}$$

$$g_2(\alpha) = 0.76 - 2.28\alpha + 3.87\alpha^2 - 2.04\alpha^3 + \frac{0.66}{(1-\alpha)^2} \tag{6}$$

where, a_o= initial crack depth, D = depth of the beam

By equating E_1 and E_2, the critical effective elastic crack length a_c can be obtained. Using the following LEFM relationship, K_{IC} and CTODc can be calculated given the geometric function (g_1) for the TPB specimen.

$$K_{IC} = 3(P_c + 0.5P_0S/L)\frac{S\sqrt{\pi a_c}g_1(a_c/D)}{2D^2t}, \tag{7}$$

where

$$g_1\left(\frac{a_c}{D}\right) = \frac{1.99-(a_c/D)(1-a_c/D)\left[2.15-3.93(a_c/D)+2.70(a_c/D)^2\right]}{\sqrt{\pi}[1+2(a_c/D)][1-(a_c/D)]^{3/2}} \tag{8}$$

(for S/D = 4.0)

$$CTOD_c = 6\left(P_c + 0.5P_0S/L\right)\frac{Sa_cg_2(a_c/D)}{ED^2t} \left[(1-\beta_0)^2 + \left[1.081 - 1.149\left(\frac{a_c}{D}\right)\right]\left(\beta_0 - \beta_0^2\right)\right]^{1/2}, \tag{9}$$

where,

$$\beta_0 = \frac{a_o}{a_c} \tag{10}$$

4 Multivariate Adaptive Regression splines (MARS)

MARS is widely accepted by researchers and practitioners for the following reasons. Firstly,(i) MARS is capable of modeling complex non-linear relationship among variables without strong model assumptions, (ii) MARS can capture the relative importance of independent variables to the dependent variable when many potential independent variables are considered and (iii) MARS does not need long training process and hence can save lots of model building time, especially when the dataset is huge. Finally, the highlighting advantage feature of MARS over other regression and classification techniques is the resulting model can be easily interpreted. MARS points out the variables that are important in developing the model. It also indicates the particular function that belongs to a specific class in case of classification when the built rules are satisfied.

In order to build a MARS are model, training data, including the input variables and the expected output targets, is required. The MARS model splits the training data into several splines on an equivalent interval basis. In each spline, MARS splits the data further into many subgroups and creates several knots, which can be located between different input variables or different intervals in the same input variable, to separate the subgroups. The MARS model approximates a regression function, called a basis function (BF), using smoothing splines to generally represent the data in each subgroup (Friedman 1991, Sephton 2001). Between any two knots, the model can characterize the data either globally or by using linear regression. The BF is unique between any two knots, and is shifted to another BF at each knot (Abraham and Steinberg 2001, Friedman 1991). The two BFs in two adjacent domains of data intersect at the knot to make model outputs continuous (Sephton 2001). Thus, MARS creates a bended regression line to fit the data from subgroup to subgroup and from spline to spline. To avoid over-fitting and over-regressing, the shortest distance between two neighboring knots is pre-determined to prevent too few data in a subgroup.

The ultimate aim of the model is to capture the relationship between the dependent variable and the independent variable from the data. In general, MARS function

can be represented by using the following equation (Firedman 1991)

$$y = \hat{f}(x) = a_0 + \sum_{m=1}^{M} a_m B_m^{(q)}(x) \tag{11}$$

where,

a_0 = coefficient of the constant basis function, or the constant term

$\{a_m\}_1^M$ = vector of coefficients of the non-constant basis functions, m= 1, 2, …, M

$B_m^{(q)}$ are the basis functions that are selected for inclusion in the model of q^{th} order

$$B_m^{(q)}(x) = \prod_{k-1}^{k_m} \left[s_{km} \cdot \left(x_{v(k,m)} - t_{km} \right) \right]_+^q \tag{12}$$

where

$B_m^{(q)}(x)$ = vector of non-constant (truncated) basis functions, or the tensor product spline basis m = number of non-constant basis functions (1, 2… M)

q = the power to which the spline is raised in order to control the degree of smoothness of the resultant function estimate, which in this case is equal to 1

'+' = denotes that only positive results of the right-hand side of the equation are considered; otherwise, the functions evaluate to 0.

s_{km} = indicates the (left/right) sense of truncation, which assumes only 2 values ($\pm$ 1), representing the standard basis function and its mirror image. For S_{km} equal to +1, the basis function will have a value x-t if x>t and 0 if x $\leq$ t. If it is -1, the basis function will have a value t-x when x<t, while 0 if x $\geq$t

$x_{v(k,m)}$ = value of the predictor

$v(k,m)$ = label of the predictor $(1 \leq v(k,m) \leq n)$

n = number of predictors

t_{km} = "knot" location on the corresponding predictor space or region, or value that defines an inflection point along the range of the predictor

K= maximum level or order of interaction, or the number of factors, in the m^{th} basis function (1, 2, …, K_m)

Basis functions are a set of functions used to represent the information contained in one or more variables. Like principal components, basis functions re-express the relationship of the predictors with the dependent variable.

Parameters of Mars can be estimated by the Penalized Least Squares (PLS) with the form:

$$P(x) = \min \sum \left(y_i - \hat{f}(x_i) \right)^2 + \lambda \int f^n(x_i) dx_i \tag{13}$$

In the above equation the first term represents the residual sum of squares and the second term represents the roughness penalty term, which is weighted by λ (known as the smoothing constant)

The penalty term is large when the integrated second derivative of the regression function $f''(x)$ is large – that is, when $f(x)$is 'rough' (with rapidly changing slope). At one extreme, when the λ is set to zero (and if all the values of x are distinct), the objective function simply interpolates the data. At the other extreme, if λ is very large, then the objective function will be selected so that its second derivative is everywhere zero, implying a globally linear least-squares fit to the data (Fox 2002).

When fitting a MARS model, knots are chosen in an iterative (recursive, i.e., from low to high interaction order) forward stepwise procedure. One of the most useful applications of variable nesting in MARS is in dealing i^{th} missing values among the independent variables. MARS creates two basis functions for any variable with missing data, one for the presence of missing values and one for the absence (Francis 2007). However, MARS does not consider interactions with missing value indicators to be genuine interactions. Thus, if MARS is directed to generate only an additive model, it may still contain interactions involving these missing value indicators (Salford Systems 2001). After over-fitting the model with so many basis functions, a backward spurning or snubbing procedure is applied in which those basis functions that contribute least to model fit are progressively removed. At this stage, a predictor variable can be dropped from the model completely if none of its basis functions contribute meaningfully to predictive performance. The sequence of models generated from this process is then evaluated using the Generalized Cross-Validation (GCV), and the model with the best predictive fit is finally selected.

The GCV can be expressed as follows

$$GCV\,(M) = \frac{\frac{1}{N}\sum_{i=1}^{N}\left[y_i - \underset{M}{\hat{f}}\,(x_i)\right]^2}{\left[1 - \frac{C(M)}{N}\right]^2} \tag{14}$$

where,

The numerator denotes lack-of-fit on the training data (sort of "bias") and the denominator accounts the (inverse) penalty for increasing model complexity C(M) (sort of "variance")

N = observations

C(M) = Cost penalty measures of a model

M = basis functions

$F_m(x_i)$= basis function model

MARS minimizes GCV (M), which reduces the bias of the model estimates but at the same time increases the variance due to additional parameters included to improve the fit of the model. Friedman and Silverman (1989) suggested using equation (13) as a lack-of-fit criterion but with an increased cost complexity function $\widetilde{C}(M)$ to reflect the additional (basis Function) parameters that, along with the expansion coefficients ($a_0,\ldots, a_M$), are being fit to the data. Such a cost complexity function can be expressed as:

$$\widetilde{C}(M) = C(M) + d.M \tag{15}$$

where

C (M) = number of parameters being fitted

M = number of non-constant basis functions in the model, which is proportional to the number of (non-linear) basis function parameters

d = cost for each basis function optimization and is a (smoothing) parameter of the procedure; larger values leads to fewer knots being placed and thereby smoother function estimates Moreover, in order to reveal considerable information about the predictive relationship between the dependent variable and a set of predictors, equation (11) can be recast into the following form:

$$\hat{f}(x) = a_0 + \sum_{K_m=1} f_i(x_i) + \sum_{K_m=2} f_{ij}(x_i, x_j) + \sum_{K_m=3} f_{ijk}(x_i, x_j, x_k) + \ldots \tag{16}$$

This is referred to as the ANOVA decomposition of the MARS model. The first sum is over all basis functions that involve only a single variable. The second sum is over all basis functions that involve exactly two variables, representing (if present) two-variable interactions. Similarly, the third sum represents (if present) the contributions from three-variable interactions and so on.

MARS can also address the missing value problems using virtual or the dummy variable skills. By allowing any arbitrary shape for the function and interactions, MARS is capable of tracking very complex data structures that hide in high dimensional frequently data. More details regarding the model building process can be found in Friedman (1991) and Salford systems (2001).

4.1 Mars based analysis

In order to predict the failure load (P_{max}) and the fracture characteristics (G_F, $CTOD_c$ and K_{Ic}) of HSC and UHSC beams, four individual MARS models have been developed. MATLAB software is used for development of MARS models.

The data that forms an input vector has different quantitative limits as shown in the Table 3 Normalization of the data is to be carried out before presenting the input

Table 3: Training Data Sets for MARS

S. No	L (mm)	A (cm^2)	a_0 (mm)	w/c	f_{ck} (MPa)	σt (MPa)	E (GPa)	P_{max} (KN)	G_F (N/m)	K_{IC} (Mpa $\sqrt{m}$)	$CTOD_C$ (mm)
1	250	25	5	0.45	57.14	3.96	35.78	2.71	115.84	1.126	0.031
2	250	25	4	0.45	57.14	3.96	35.78	2.62	123.31	1.129	0.03
3	250	25	10	0.45	57.14	3.96	35.78	1.98	91.12	1.092	0.0183
4	250	25	9	0.45	57.14	3.96	35.78	1.98	86.65	1.08	0.0186
5	250	25	10	0.45	57.14	3.96	35.78	1.84	74.32	1.083	0.0178
6	250	25	16	0.45	57.14	3.96	35.78	1.14	55.18	0.916	0.0081
7	250	25	15	0.45	57.14	3.96	35.78	1.42	68.61	0.902	0.008
8	500	50	9	0.45	57.14	3.96	35.78	4.53	144.02	1.348	0.049
9	500	50	10	0.45	57.14	3.96	35.78	4.10	130.26	1.349	0.0485
10	500	50	18	0.45	57.14	3.96	35.78	3.79	92.72	1.174	0.035
11	500	50	19	0.45	57.14	3.96	35.78	3.63	115.42	1.173	0.0345
12	500	50	28	0.45	57.14	3.96	35.78	2.58	89.12	0.984	0.0149
13	1000	100	19	0.45	57.14	3.96	35.78	7.27	165.25	1.467	0.1026
14	1000	100	19	0.45	57.14	3.96	35.78	7.32	146.28	1.461	0.1
15	1000	100	19	0.45	57.14	3.96	35.78	6.99	148.25	1.456	0.098
16	1000	100	39	0.45	57.14	3.96	35.78	6.01	135.85	1.224	0.0601
17	1000	100	39	0.45	57.14	3.96	35.78	6.32	140.56	1.201	0.06
18	1000	100	58	0.45	57.14	3.96	35.78	4.54	115.12	1.012	0.0281
19	1000	100	60	0.45	57.14	3.96	35.78	4.70	104.22	0.998	0.026
20	250	25	5	0.33	87.71	15.38	37.89	4.20	4157.28	7.984	0.3434
21	250	25	5	0.33	87.71	15.38	37.89	4.15	4102.2	7.941	0.321
22	250	25	10	0.33	87.71	15.38	37.89	3.37	3464.6	7.398	0.2213
23	250	25	10	0.33	87.71	15.38	37.89	3.26	3880.1	7.362	0.218
24	250	25	15	0.33	87.71	15.38	37.89	2.79	3301.2	6.961	0.098
25	250	25	15	0.33	87.71	15.38	37.89	2.88	3410	6.981	0.1
26	250	25	20	0.33	87.71	15.38	37.89	1.98	2892.06	6.118	0.053
27	250	25	20	0.33	87.71	15.38	37.89	2.05	2988.52	6.3	0.051
28	500	50	10	0.33	87.71	15.38	37.89	8.35	4811	8.479	0.456
29	500	50	10	0.33	87.71	15.38	37.89	8.20	4200.1	8.453	0.45
30	500	50	20	0.33	87.71	15.38	37.89	5.10	4516.1	7.401	0.3268
31	500	50	20	0.33	87.71	15.38	37.89	4.99	4266.5	7.386	0.32
32	500	50	20	0.33	87.71	15.38	37.89	5.07	3828.57	7.365	0.318
33	500	50	30	0.33	87.71	15.38	37.89	3.80	3579.89	6.682	0.203
34	500	50	30	0.33	87.71	15.38	37.89	3.79	3865.2	6.701	0.206
35	500	50	40	0.33	87.71	15.38	37.89	2.99	3970.95	6.201	0.093
36	500	50	40	0.33	87.71	15.38	37.89	3.08	3406.67	6.196	0.09
37	250	25	4	0.23	122.52	20.65	42.987	9.99	10349.24	12.601	0.433
38	250	25	5	0.23	122.52	20.65	42.987	10.01	10376.22	12.652	0.44
39	250	25	10	0.23	122.52	20.65	42.987	7.81	8308.49	11.762	0.281
40	250	25	9	0.23	122.52	20.65	42.987	7.43	7900	11.801	0.279
41	250	25	15	0.23	122.52	20.65	42.987	6.20	6925.54	11.092	0.141
42	250	25	15	0.23	122.52	20.65	42.987	5.99	6694.51	11	0.142
43	250	25	20	0.23	122.52	20.65	42.987	4.07	4386.6	7.581	0.0875
44	250	25	19	0.23	122.52	20.65	42.987	3.99	4306.29	7.412	0.0861
45	250	25	20	0.23	122.52	20.65	42.987	4.18	4511.36	7.51	0.085
46	400	40	9	0.23	122.52	20.65	42.987	14.23	11557.07	13.541	0.483
47	400	40	8	0.23	122.52	20.65	42.987	13.98	11354.02	13.582	0.49
48	400	40	16	0.23	122.52	20.65	42.987	10.85	8888.75	11.949	0.3898
49	400	40	15	0.23	122.52	20.65	42.987	10.62	8700.84	11.892	0.383
50	400	40	25	0.23	122.52	20.65	42.987	7.58	7145.19	11.201	0.2515
51	400	40	24	0.23	122.52	20.65	42.987	7.61	7171.63	11.221	0.249
52	400	40	32	0.23	122.52	20.65	42.987	5.56	5021.25	8.471	0.1216
53	400	40	31	0.23	122.52	20.65	42.987	5.60	5058.14	8.45	0.12
54	650	65	13	0.23	122.52	20.65	42.987	19.49	12052.38	13.984	0.581
55	650	65	12	0.23	122.52	20.65	42.987	19.31	11944.13	13.801	0.563
56	650	65	25	0.23	122.52	20.65	42.987	13.37	8076	12.013	0.3069
57	650	65	25	0.23	122.52	20.65	42.987	13.51	8892.69	12	0.301
58	650	65	39	0.23	122.52	20.65	42.987	10.12	6965.9	11.321	0.181
59	650	65	39	0.23	122.52	20.65	42.987	10.30	7085.13	11.103	0.172
60	650	65	52	0.23	122.52	20.65	42.987	7.46	5919.23	9.691	0.094
61	650	65	52	0.23	122.52	20.65	42.987	7.69	6109.05	9.598	0.093

Note of table 3: L- length, A- c/s area, a_0- Notch depth, w/c-Water- cementations material ratio, SP- SuperPlasticizer, fck-compressive strength, σ_t-Split tensile strength, E- modulus of elasticity, P_{max}- Failure load, G_F- Fracture energy, K_{IC}- critical stress intensity factor, $CTOD_C$- Critical crack tip opening displacement.

patterns to the MARS. Equation 16 is used for the linear normalization of the data to the data values between 0 and 1.

$$x_i^n = \frac{x_i^a - x_i^{\min}}{x_i^{\max} - x_i^{\min}} \tag{17}$$

where, x_i^a and x_i^n are the i^{th} components of the input vector before and after normalization, respectively, and $x_i^{\max}$ and $x_i^{\min}$ are the maximum and minimum values of all the components of the input vector before the normalization.

Model I Failure load (P_{max})

The MARS equation for the prediction of failure load is given by equation no 17. It can be directly identified that the number of interaction effects and, in particular, interactions between efforts (as captured by basis function $B_3(x)$). Such interactions can be seen in equation (17), when basis functions are part of the definition of other basis functions, e.g., $B_3(x)$ in $B_6(x)$, $B_7(x)$ etc.

The presence of many such interactions suggests that the model is far from being additive and those interactions will play an important role in building an accurate model for code inspections. The user defined basis functions for over fitting the model was limited to 32 basis functions and the allowable highest degree of interaction was set to 2. The final model had 18 Basis functions as listed below. Thus for this model equation (11) becomes

$$y = \mathrm{Pmax} = 0.329 + \sum_{m=1}^{18} a_m B_m^{(1)}(x) \tag{18}$$

where,

The ANOVA decomposition is specified in row wise for each ANOVA function. The columns represent summary quantities for corresponding ones. The first column lists the function number. The second gives the standard deviation (STD) of the function. This gives indication of its (relative) importance to the overall model and can be interpreted in a manner similar to a standard regression coefficient in a linear model. The third column provides another indication of the importance of the corresponding

ANOVA function, by listing the GCV score for a model with the entire basis functions corresponding to that particular ANOVA function removed. This can be used

Basis function $B_m^{(1)}(x)$	**Equation**	**Co-efficient** ($\mathbf{a}_m$)
$B_1(x)$	max (0, f_{ck} -0.468)	1.453
$B_2(x)$	max (0, 0.468 - f_{ck})	-0.354
$B_3(x)$	max(0, L -0.333)	-0.501
$B_4(x)$	max(0, 0.333 -L)	-0.899
$B_5(x)$	max(0, a_0 -0.222)	-2.213
$B_6(x)$	$B_3(x)$ * max(0, a_0 -0.370)	-7.0594
$B_7(x)$	$B_3(x)$ * max(0, 0.370 - a_0)	6.209
$B_8(x)$	$B_5(x)$ * max(0, L -0.2)	6.423
$B_9(x)$	$B_4(x)$ * max(0, a_0 -0.185)	3.433
$B_{10}(x)$	$B_4(x)$ * max(0, 0.185 - a_0)	1.412
$B_{11}(x)$	$B_5(x)$ * max(0, w/c -0)	0.692
$B_{12}(x)$	$B_4(x)$ * max(0, E -0.293)	-1.097
$B_{13}(x)$	$B_4(x)$ * max(0, 0.293 -E)	1.0686
$B_{14}(x)$	max(0, 0.222 - a_0) * max(0, f_{ck} -0.468)	5.267
$B_{15}(x)$	max(0, a_0 -0.370)	0.786
$B_{16}(x)$	$B_1(x)$ * max(0, a_0 -0.389)	2.817
$B_{17}(x)$	$B_1(x)$ * max(0, 0.389 - a_0)	-3.603
$B_{18}(x)$	$B_1(x)$ * max(0, a_0 -0.185)	-2.945

to judge whether this ANOVA function is making an important contribution to the model, or whether it just slightly helps to improve the global GCV score. The fourth column gives the number of basis functions comprising the ANOVA and the last column of Table 4 gives the particular predictor variables associated with the ANOVA function.

Table 4: ANOVA decomposition – Failure load (P_{max})

Func.	STD	GCV	#basis	variable(s)
1	0.127	0.102	2	L
2	0.329	0.31	2	a_0
3	0.421	0.483	2	f_{ck}
4	0.273	0.201	5	L & a_0
5	0.106	0.028	2	L & E
6	0.107	0.027	1	a_0 & w/c
7	0.144	0.07	4	a_0 & f_{ck}

The value of coefficient of correlation (R) is determined by using the following

formula

$$R = \frac{\sum_{i=1}^{n} \left(E_{ai} - \overline{E}_a\right)\left(E_{pi} - \overline{E}_p\right)}{\sqrt{\sum_{i=1}^{n} \left(E_{ai} - \overline{E}_a\right)} \sqrt{\sum_{i=1}^{n} \left(E_{pi} - \overline{E}_p\right)}} \tag{19}$$

where E_{ai} and E_{pi} are the actual and predicted values, respectively, $\overline{E}_a$ and $\overline{E}_p$ are mean of actual and predicted E values corresponding to n patterns.

Model II- Fracture Energy (G_F)

The predicted model for $G_F$is given below

$$y = G_F = 0.305 + \sum_{m=1}^{8} a_m B_m^{(1)}(x) \tag{20}$$

where

Basis function $B_m^{(1)}(x)$	**Equation**	**Co-efficient (a_m)**
$B_1(x)$	max(0, w/c -0.454)	-0.551
$B_2(x)$	max(0, 0.455-w/c) * max(0, a_0 -0.389)	-8.782
$B_3(x)$	max(0, 0.455-w/c) * max(0, 0.389- a_0)	4.716
$B_4(x)$	max(0, 0.455-w/c) * max(0, L -0.2)	0.362
$B_5(x)$	max(0, 0.455-w/c) * max(0, 0.2 -L)	-2.463
$B_6(x)$	$B_4(x)$ * max(0, a_0 -0.370)	13.455
$B_7(x)$	$B_4(x)$ * max(0, 0.370- a_0)	4.498
$B_8(x)$	max (0, 0.455-w/c) * max(0, a_0 -0.185)	3.307

Table 5 shows the details ANOVA decomposition

Table 5: ANOVA decomposition - Fracture energy

Func.	STD	GCV	#basis	variable(s)
1	0.135	0.039	1	w/c
2	0.084	0.015	2	L & w/c
3	0.31	0.127	3	a_0 & w/c
4	0.196	0.054	2	L, a_0 & w/c

Model III – Critical Stress Intensity Factor (K_{IC})

The predicted model for $K_{IC}$is given below.

$$y = \mathrm{K_{IC}} = 0.421 + \sum_{m=1}^{14} a_m B_m^{(1)}(x) \tag{21}$$

where,

Basis function $B_m^{(1)}(x)$	**Equation**	**Co-efficient (a_m)**
B_1(x)	max(0, w/c -0.455)	-0.767
B_2(x)	max(0, 0.454-w/c)	0.835
B_3(x)	B_2(x) * max(0, a_0 -0.389)	-1.759
B_4(x)	B_2(x)* max(0, 0.389 - a_0)	-3.015
B_5(x)	B_2(x)* max(0, L -0.2)	0.554
B_6(x)	B_2(x)* max(0, 0.2 -L)	-0.201
B_7(x)	max(0, a_0 -0.370)	0.250
B_8(x)	max(0, 0.370- a_0)	0.690
B_9(x)	B_7(x)* max(0, L -0.333)	-0.347
B_{10}(x)	B_7(x)* max(0, 0.333-L)	-13.071
B_{11}(x)	B_8(x) * max(0, w/c -0.455)	-0.983
B_{12}(x)	B_8(x)* max(0, 0.455-w/c)	3.019
B_{13}(x)	max(0, 0.2 –L)	-0.478
B_{14}(x)	B_{13}(x) * max(0, 0.684-σ_t)	0.319

Table 6 shows the details of ANOVA decomposition for K_{IC}model.

Table 6: ANOVA decomposition – K_{IC}

Func.	STD	GCV	#basis	variable(s)
1	0.046	0.014	1	L
2	0.076	0.046	2	a_0
3	0.339	0.147	2	w/c
4	0.055	0.008	2	L & a_0
5	0.03	0.01	2	L & w/c
6	0.014	0.009	1	L & σ_t
7	0.079	0.014	4	a_0& w/c

Model IV – Critical Crack Tip Opening Displacement ($CTOD_C$)

The predicted model for $CTOD_c$is given below

$$y = CTOD_C = 0.387 + \sum_{m=1}^{14} a_m B_m^{(1)}(x) \tag{22}$$

where,

Basis function $B_m^{(1)}(x)$	**Equation**	**Co-efficient (a_m)**
B_1(x)	max(0, w/c -0.455)	-0.626
B_2(x)	max(0, 0.455-w/c)	0.183
B_3(x)	B_2(x) * max(0, a_0 -0.389)	-4.272
B_4(x)	B_2(x) * max(0, 0.389- a_0)	2.994
B_5(x)	max(0, a_0 -0.222)	-0.283
B_6(x)	max(0, 0.222- a_0)	2.638
B_7(x)	max(0, L -0.2)	0.224
B_8(x)	max(0, 0.2 -L)	-1.488
B_9(x)	B_6(x) * max(0, f_{ck} -0.468)	-17.852
B_{10}(x)	B_6(x) * max(0, 0.468- f_{ck})	-5.428
B_{11}(x)	B_8(x) * max(0, w/c -0.455)	2.391
B_{12}(x)	max (0, 0.455-w/c) * max(0, L -0.2) * max(0, a_0 -0.370)	9.224
B_{13}(x)	max (0, 0.455-w/c) * max(0, L -0.2) * max(0, 0.370- a_0)	12.822
B_{14}(x)	B_2(x) * max (0, 0.185- a_0)	19.470

Table 7 shows the details of ANOVA decomposition for $CTOD_c$.

Table 7: ANOVA decomposition -$CTOD_c$

Func.	STD	GCV	#basis	variable(s)
1	0.185	0.082	2	L
2	0.223	0.098	2	a_0
3	0.183	0.07	2	w/c
4	0.084	0.02	1	L & w/c
5	0.529	0.46	3	a_0 & w/c
6	0.471	0.479	2	a_0 & f_{ck}
7	0.15	0.043	2	L, a_0 & w/c

Table 8 shows the complete statistics for all the developed MARS models. The GCV was computed using the equation 13 and the coefficient of correlation (R) was computed using equation 18.

Table 8: Testing of MARS

MARS results		P_{max}	G_F	K_{IC}	$CTOD_C$
User defined max. no. of Basis functions		32	12	20	18
Interactions Ratio allowed		2	4	2	4
Final no. of basis functions		18	8	14	14
Mean Square Error (MSE)	Train	7.48E-05	4.51E-04	1.73E-04	6.79E-04
	Test	9.77E-04	0.0011	0.0047	0.004
Root Mean Square Error (RMSE)		0.0313	0.0335	0.0683	0.0629
Generalized Cross Validation		3.75E-04	0.0011	9.64E-04	0.0038
Coefficient of correlation (R)	Train	0.998	0.9976	0.9988	0.9947
	Test	0.9993	0.9977	0.9993	0.996

Table 9: Test results of MARS model ($P_{max}$and G_F)

L (mm)	A (cm^2)	a_0 (mm)	w/c	f_{ck} (MPa)	σ_t (MPa)	E (GPa)	P_{max} (kN)		G_F(N/m)	
							Exptl.	MARS	Exptl	MARS
250	25	4	0.45	57.14	3.96	35.78	2.412	2.161	114.9	101.6
250	25	17	0.45	57.14	3.96	35.78	1.321	1.248	47.4	101.6
500	50	29	0.45	57.14	3.96	35.78	2.575	2.323	96.2	101.6
500	50	28	0.45	57.14	3.96	35.78	2.321	2.301	100.3	101.6
500	50	10	0.33	87.71	15.38	37.89	8.102	8.046	4142.2	4351.2
1000	100	40	0.45	57.14	3.96	35.78	6.278	6.204	110.2	101.6
500	50	10	0.45	57.14	3.96	35.78	4.312	4.318	137.0	101.6
250	25	10	0.33	87.71	15.38	37.89	3.121	3.062	3763.1	3838.7
650	65	51	0.23	122.52	20.65	42.987	7.312	7.233	5806.5	5719.1
500	50	30	0.33	87.71	15.38	37.89	3.991	4.085	4623.5	3666.7
250	25	9	0.23	122.52	20.65	42.987	7.667	8.169	8155.0	8489.0
250	25	14	0.23	122.52	20.65	42.987	6.128	5.868	6844.0	6560.3
400	40	8	0.23	122.52	20.65	42.987	14.08	14.198	11435.2	11489.8
400	40	16	0.23	122.52	20.65	42.987	10.514	10.715	8613.2	8459.5
650	65	24	0.23	122.52	20.65	42.987	13.498	13.723	8155.1	8114.3
650	65	13	0.23	122.52	20.65	42.987	19.126	19.489	11829.1	11818.5
650	65	39	0.23	122.52	20.65	42.987	10.013	10.212	6889.1	7057.5
250	25	5	0.23	122.52	20.65	42.987	10.136	10.012	10504.7	10358.7
250	25	20	0.33	87.71	15.38	37.89	2.102	1.928	2894.0	3471.1
400	40	31	0.23	122.52	20.65	42.987	5.312	5.443	4797.2	4809.5
250	25	5	0.33	87.71	15.38	37.89	4.101	4.067	4056.4	4153.3
500	50	40	0.33	87.71	15.38	37.89	3.194	2.965	2897.9	3042.3
1000	100	58	0.45	57.14	3.96	35.78	4.412	4.353	111.9	101.6
400	40	25	0.23	122.52	20.65	42.987	7.31	6.997	6887.1	6986.8
500	50	18	0.45	57.14	3.96	35.78	3.87	3.680	105.3	101.6
250	25	15	0.33	87.71	15.38	37.89	2.841	2.605	3685.1	3600.7

Table 10: Test results of MARS model (K_{IC} and $CTOD_c$)

L (mm)	A (cm^2)	a_0 (mm)	w/c	f_{ck} (MPa)	σ_t (MPa)	E (GPa)	K_{IC} (Mpa $\sqrt{m}$)		$CTOD_C$(mm)	
							Exptl.	MARS	Exptl.	MARS
250	25	4	0.45	57.14	3.96	35.78	1.121	1.0176	0.029	0.026
250	25	17	0.45	57.14	3.96	35.78	0.923	1.0267	0.008	0.011
500	50	29	0.45	57.14	3.96	35.78	0.998	1.0059	0.015	0.013
500	50	28	0.45	57.14	3.96	35.78	0.979	0.9956	0.015	0.016
500	50	10	0.33	87.71	15.38	37.89	8.462	8.5571	0.432	0.402
1000	100	40	0.45	57.14	3.96	35.78	1.234	1.0267	0.062	0.065
500	50	10	0.45	57.14	3.96	35.78	1.356	1.4699	0.051	0.057
250	25	10	0.33	87.71	15.38	37.89	7.312	7.2664	0.213	0.213
650	65	51	0.23	122.52	20.65	42.987	9.601	9.6302	0.091	0.078
500	50	30	0.33	87.71	15.38	37.89	6.721	6.5705	0.206	0.186
250	25	9	0.23	122.52	20.65	42.987	11.857	11.9744	0.283	0.293
250	25	14	0.23	122.52	20.65	42.987	11.183	11.1451	0.145	0.140
400	40	8	0.23	122.52	20.65	42.987	13.655	13.536	0.494	0.502
400	40	16	0.23	122.52	20.65	42.987	11.901	12.174	0.38	0.376
650	65	24	0.23	122.52	20.65	42.987	11.98	12.0755	0.289	0.311
650	65	13	0.23	122.52	20.65	42.987	13.882	13.8742	0.571	0.572
650	65	39	0.23	122.52	20.65	42.987	11.201	11.0854	0.162	0.184
250	25	5	0.23	122.52	20.65	42.987	12.716	12.6366	0.443	0.432
250	25	20	0.33	87.71	15.38	37.89	6.317	6.6781	0.055	0.058
400	40	31	0.23	122.52	20.65	42.987	8.463	8.6686	0.119	0.110
250	25	5	0.33	87.71	15.38	37.89	7.912	8.0206	0.33	0.348
500	50	40	0.33	87.71	15.38	37.89	6.214	6.2699	0.096	0.135
1000	100	58	0.45	57.14	3.96	35.78	1	1.1057	0.027	0.011
400	40	25	0.23	122.52	20.65	42.987	11.198	10.8392	0.25	0.229
500	50	18	0.45	57.14	3.96	35.78	1.176	1.1394	0.036	0.045
250	25	15	0.33	87.71	15.38	37.89	6.993	6.5692	0.101	0.092

Note of table 10: L- length, A- c/s area, a_0- Notch depth, w/c-Water- cementations material ratio, SP- SuperPlasticizer, f_{ck} -compressive strength, σ_t-Split tensile strength, E- modulus of elasticity, P_{max}- Failure load, G_F- Fracture energy, K_{IC}- critical stress intensity factor, $CTOD_C$- Critical crack tip opening displacement.

On successful development of MARS model with 61 dataset, the model is verified with remaining 26 dataset. The results are shown in Tables 9 and 10. The output vector obtained from the MARS model is a normalized data and hence, the normalized data is reverted to its actual value by using equation (23).

$$x_i^a = x_i^n \left(x_i^{\max} - x_i^{\min}\right) + x_i^{\min} \tag{23}$$

where, x_i^n is the normalized result obtained after the test for the ith component. $x_i^a$is the actual result obtained for ith componenet, and $x_i^{\max}$ and $x_i^{\min}$are the maximum

and minimum values of all the compoents of the corresponding input vector before the normalization.

From Tables 7 and 8, it can be observed that the predicted values of $P_{max,}G_{F,}K_{Ic}$ and $CTOD_c$, are in very good agreement with each other. Figs. 1 to 4 show the comparison of predicted and experimental P_{max}, G_F, K_{IC} and $CTOD_C$ respectively. From Figures 1 to 4, it can be observed that the developed models are robust and reliable.

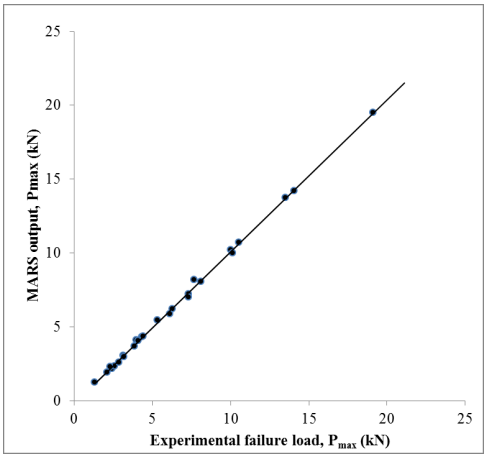

Figure 1: Experimental vs predicted failure load (P_{max})

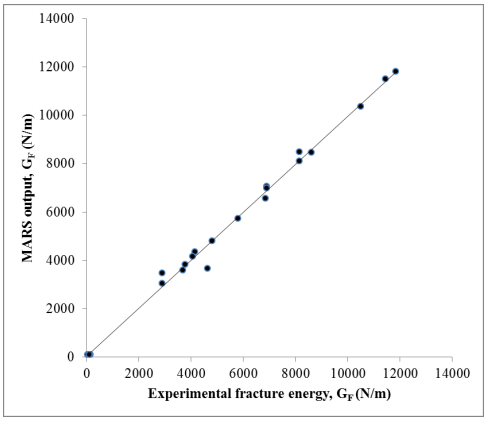

Figure 2: Experimental vs predicted G_F

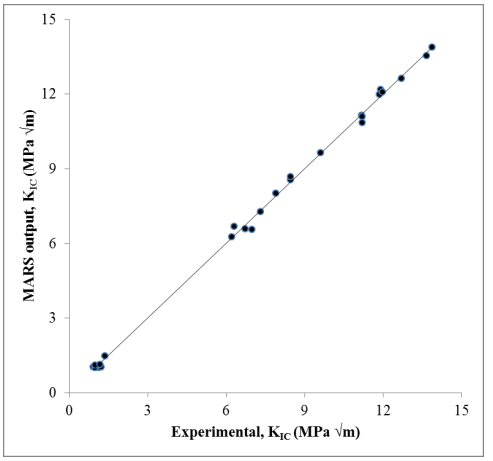

Figure 3: Experimental vs predicted K_I

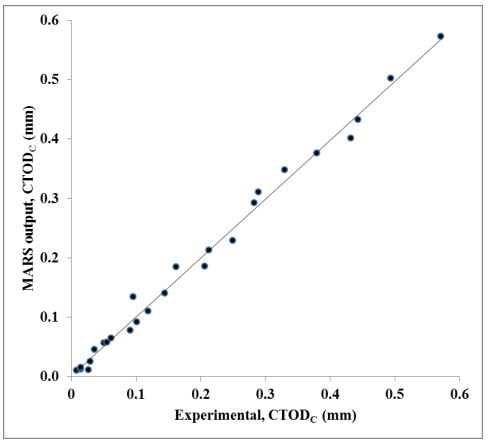

Figure 4: Experimental vs predicted $CTOD_c$

5 Summary and conclusion

Fracture mechanics based MARS model has been developed to predict the fracture characteristics of HSC and UHSC. Fracture characteristics include fracture energy (G_F), critical stress intensity factor (K_{IC}) and critical crack tip opening displacement ($CTOD_c$). MARS model has also been developed to predict the failure loads under the three point bending test for HSC and UHSC beam specimens. Characterization of mix of high strength and ultra high strength concrete has been described. An overview of experimental details of beams tested under static loading has been

shown and methodologies for evaluation of fracture energy, critical stress intensity factor and critical crack tip opening displacement have been outlined. MARS establishes a relationship between a set of predicators and dependent variables. MARS is based on a divide and conquers strategy partitioning the training data sets into separate region; each gets its own regression line Four MARS models have been developed using MATLAB software for training and prediction of the three fracture parameters and failure load. MARS has been trained with about 70% of the total 87 data sets and tested with about 30% of the total data sets. It is observed that the predicted values of failure load, facture energy, critical stress intensity factor and critical crack tip opening displacement are in good agreement with those of the experimental values. The developed models will be readily useful for prediction of fracture parameters of HSC and UHSC beams.

Acknowledgements

We acknowledge with thanks the valuable technical suggestions and support provided by the colleagues of Computational Structural Mechanics Group of CSIR-SERC. The help and support provided by the staff of Advanced Materials Laboratory, CSIR-SERC to carry out the experiments is greatly acknowledged. This paper is being published with the permission of the Director, CSIR- SERC, Chennai, India.

References

Adeli, H. (2001): Neural networks in civil engineering: 1989-2001 *Computer-Aided Civil and Infrastructure Engineering*, vol.16, pp.126-142.

Attoh-Okine, N.O.; Cooger, K.; Mensah, S. (2009): Multivariate adaptive regression (MARS) and hinged hyperplanes (HHP) for doweled pavement performance modelling. *Construction and Building Materials*, vol.23, pp.3020–3023.

Abraham, A.; Steinberg D (2001): MARS: still an alien planet in soft computing? In: International Conference on Computational Science (Alexandrov V N; Dongarra J; Juliano B A; Renner R S; Tan C J K, eds) Lecture Notes in Computer Science, Springer-Verlag, Heidelberg, Germany, 2074, pp. 235–244.

Barenblatt, G. I. (1959): The formation of equilibrium cracks during brittle fracture: general ideas and hypotheses, axially symmetric cracks. *Appl Math Mech*, vol.23, pp.622–36.

Bazant, Z. P. (2000): Size effect. *Int J Solid Struct,* vol.3, pp.69–80.

Bhashya, V.; Ramesh, G.; Sundar Kumar, S.; Bharatkumar, B. H.; Krishnamoorthy, T. S.; Iyer, N. R. (2011): Experimental and Analytical Studies on

Concrete Cylinders Wrapped with Fiber Reinforced Polymer. *Computers Materials and Continua,* vol.25, no.1, pp.47.

Chou Lee, T.S.; Shao, Y. E.; Chen, I.F. (2004): Mining the breast cancer pattern using artificial neural networks and multivariate adaptive regression splines. *Expert Systems with Applications,* vol.27, no.1, pp.133–142.

Dugdale, D. S. (1960): Yielding of steel sheets containing slits. *J Mech Phys Solids*, vol.8, pp.100–4.

De Veaux, R.D.; Psichogios,D.C.; Ungar, L.H. (1993): A comparison of comparsion of two nonparametric estimation schemes: MARS and neural networks. *Comput. Chem. Eng.,* vol.17, no.8, pp.819-837.

Dong, L.; Atluri, S. N. (2013): Fracture & Fatigue Analyses: SGBEM-FEM or XFEM? Part 1: 2D Structures. *CMES: Computer Modeling in Engineering & Sciences,* vol.90, no.2, pp.91-146.

Dong, L.; Atluri, S. N. (2013): Fracture & Fatigue Analyses: SGBEM-FEM or XFEM? Part 2: 3D solids. *CMES: Computer Modeling in Engineering & Sciences,* vol.90, no.5, pp.379-413.

Ekman, T.; Kubin, G. (1999): Nonlinear prediction of mobile radio channels: measurements and Mars model designs in IEEE International Conference on Acoustics. *Speech and Signal Processing,* pp.2667-2670.

Fox, J. (2002): Nonparametric Regression. Appendix to An R and S-PLUS Companion to Applied Regression

Francis, Louise. (2007): Martian Chronicles: Is MARS Better Than Neural Networks? Retrieved.

Friedman, J. H. (1991): Multivariate adaptive regression splines The Annals of Statistics, vol.19, no.1, pp.1-67.

Friedman, J. H.; Silverman, B. W. (1989): Flexible parsimonious smoothing and additive modelling. *Technometrics,* vol.31, pp.3-39.

Goltermann, P.; Johansen, V.; Palbol, L. (1997): Packing of Aggregates: An Alternate Tool to Determine the Optimal Aggregate Mix. *ACI Material Journal,* pp. 435-443.

Hillerborg, A.; Modeer, M.; Petersson, P.E. (1976): Analysis of crack formation and crack growth in concrete by means of fracture mechanics and finite elements. *Cem. Concr. Res.*, vol.6, pp.773–782.

Jenq, Y. S.; Shah, S.P. (1985): A two parameter fracture model for concrete. *Journal of Engineering Mechanics,* vol.111, no.4, pp.1227-1241.

Jin, R.; Chen, W.; Simpson, T.W. (2000): Comparative Studies of Metamodelling

Techniques Under Multiple Modelling Criteria American institute of Aeronautics and Astronautics AIAA-pp.2000-4801.

Karihaloo, B.L.(1995): *Fracture Mechanics and structural Concrete.* Longman Scientific & Technical, U.K.

Leathwick, J. R.; Rowe, D.; Richardson, J.; Elith, J.; Hastie, T. (2005): Using multivariate adaptive regression splines to predict the distributions of New Zealand's freshwater diadromous fish. *Freshwater Biology*, vol.50, no.12, pp. 2034–2052.

Loizos, A.; Karlaftis, M. G. (2006): Neural networks and non-parametric statistical models: A comparative analysis in pavement condition analysis A.*dvances and Applications in Statistics*, vol.6, no.1, pp.87-110.

Mallick, B.K.; Denison, D.G.T.; Smith, A.F.M. (1997): Bayesian survival analysis using a MARS model Technical Report, Imperical College, London.

Murthy, A. R. C.; Palani, G. S.; Iyer, N. R.; Prasad, B. R.; Pavan, M. S.; Gopinath, S. (2010): Fracture Analysis of Concrete Structural Components Accounting for Tension Softening Effect. Computers. *Materials & Continua* (CMC), vol.19, no.2, pp.135-154.

Murthy, A. R.; Iyer, N. R.; Prasad, B. R. (2012): Fatigue Crack Growth Study and Remaining Life Assessment of High Strength and Ultra High Strength Concrete Beams. *Computer Modeling in Engineering & Sciences,* vol.89, no.6, pp.457-478.

Prasad, A.M.; Iverson, L.R. (2000): Predictive vegetation mapping using a custom built model-chooser; comparison of regression tree analysis and multivariate adaptive regression splines in 4^{th} international conference on integrating GIS and environmental modelling (GIS/EM4): Problems, prospects and research needs, Banf, Alberta, Canada.

Richard, P.; Cheyrezy, M. H. (1994): Reactive powder concretes with high ductility and 200–800 MPa compressive strength. *ACI SP144-24(1),* vol.144, pp.507–18.

Richard, P.; Cheyrezy, M. H. (1995): Composition of reactive powder concretes. *Cem. Concr. Res.*, vol.25, no.7, pp.1501-1511.

Riedi, M. (1997): Modeling segmental duration with multivariate adaptive regression splines. *Proc., 5th European Conference on Speech Communication and Technology* (EUROSPEECH 97), ESCA, Rhodes, Greece, pp.2627-2630.

RILEM FMC-50 (1985): Determination of the fracture energy of mortar and concrete by means of three-point bend tests on notched beams. *Material & Structures*, vol.18, no.4, pp. 287–290.

Sephton, P. (2001): Forecasting Recessions: Can We Do Better on MARS(™)?

Review (Federal Reserve Bank of St. Louis) , (March/April), pp.39-49.

Salford Systems, Inc. 2001. "MARSTM User Guide".

Vidoli, F. (2011): Evaluating the water sector in Italy through a two stage method using the conditional robust nonparametric frontier and multivariate adaptive regression splines. *European Journal of Operational Research,* vol.212, pp.583–595.

Yang, C.C.; Prasher, S.O.; Lacroix, R.; Kim. S.H. (2003): A Multivariate Adaptive Regression Splines Model for Simulation of Pesticide Transport in Soils. *Biosystems Engineerig (sciencedirect.com),* vol.86, no.1, pp.9-15.

York, T.P.; Eaves, L.J. (2001): Common disease analysis using multivariate adaptive splines (MARS): genetic analysis workshop 12 simulated sequence data. *Genet. Epidemiol.*, vol.21, pp.649-654.

Yu, Z.; Sun, M.; Zheng, S.; Liang, L. (2010): Fatigue Properties of RPC under Cyclic Loads of Single-stage and Multi-level Amplitude. *Journal of Wuhan University of Technology-Material Science Ed.,* pp.167-173.

Zhou, Y.; Leung. H. (2007): Predicting object-oriented software maintainability using multivariate adaptive regression splines. *The Journal of Systems and Software,* vol.80, pp.1349–1361.